

Yield and Fracture Mechanisms in ABS

C. C. CHEN* and J. A. SAUER, *Rutgers University,
New Brunswick, New Jersey*

Synopsis

The deformation and fracture characteristics of ABS have been investigated under tension, compression, and tension-compression fatigue cycling. The behavior of the rubber-modified polymer is compared with that of unmodified styrene-acrylonitrile copolymer. The dispersed rubber particles in ABS cause extensive plastic deformation of the matrix material, markedly reduce the compressive yield stress, and, under tensile loading, cause yielding rather than early fracture. Under alternating stress conditions crazes occur sooner and lead to earlier craze breakdown, crack development, and reduced lifetime to fracture. The influence of rate of loading has been studied under applied tension and under fatigue cycling. The tensile yield stress varies linearly with the log of the strain rate in accord with the Eyring rate equation and, from the measured slope, the activation volume is estimated to be 2.2 nm^3 . The time to fatigue fracture reduces significantly with increasing frequency while cycles to fracture increase at a modest rate. Fatigue failure in ABS is not a cycle-dependent process, nor is it in accord with a damage accumulation model, but it more nearly resembles the former. The influence of a dispersed rubber phase, and of loading rate, on fracture surface morphology is discussed.

INTRODUCTION

It is well established that the impact toughness of polymers can be appreciably enhanced by incorporation of grafted rubber particles.^{1,2} Two specific examples of this are high-impact polystyrene (HIPS), consisting of butadiene particles in polystyrene (PS), and acrylonitrile-butadiene-styrene (ABS) containing dispersed rubber particles in a styrene-acrylonitrile (SAN) matrix. When these materials are subject to increasing tensile or compressive stress the dispersed elastomeric particles act as stress concentrators and induce the matrix material to develop localized deformation zones throughout the volume of the sample at relatively low values of applied stress. Hence, although the modulus and the yield, or craze, stress are reduced by the presence of the rubber phase, the strain to fracture and the toughness are increased.

The situation is less clear relative to the influence of the rubber phase on resistance to fracture under alternating stress. In experiments on precracked specimens, it is found that rubber modification improves fatigue performance by reducing the fatigue crack propagation (FCP) rate³; but, in fatigue tests on unnotched, smooth specimens, PS was found to have a greater average fatigue life than HIPS^{4,5} and SAN had a higher fatigue life than ABS.⁶ Hence, in these latter tests, rubber modification was detrimental to fatigue performance.

The present report is a continuation of research investigations concerning the influence of a dispersed elastomeric phase on deformation and fracture.⁴⁻⁷

* Current address: Ethicon Inc. Somerville, NJ.

In this study, we have investigated deformation modes and mechanical behavior of a typical ABS polymer subject to three different applied stress loading patterns, viz., simple tension, simple compression, and sinusoidal tension-compression fatigue cycling. The results obtained on the rubber-modified polymer are compared with those obtained on two grades of unmodified SAN polymer. Another phase of this study is concerned with the influence of rate of loading on the performance of ABS specimens subject to either uniaxial tension or to fatigue cycling. The influence of strain rate on tensile yield stress and on fracture surface morphology is discussed. For samples subject to fatigue cycling, the influence of test frequency is examined over a 1000-fold range, on both the time to fracture and on the cycles to fracture. Comparisons are given, wherever applicable, with existing literature data. From these results, it may be shown that the fatigue failure of ABS is neither a stress-activated damage accumulation process nor a cycle-dependent process, but that it contains elements of both.

EXPERIMENTAL

The ABS samples for testing were machined from rods of a general purpose grade (Borg-Warner). Thin films of this polymer were examined by transmission electron microscopy (TEM) and a broad distribution of rubber particle sizes was observed, with diameters ranging from 0.04 to about 1.0 μm .⁸ The two SAN materials, obtained in pellet form from the Dow Chemical Co., had an acrylonitrile content of 30%. One, designated SAN-B had a weight-average molecular weight of 1.3×10^5 and the other, designated SAN-C, had a higher molecular weight of 1.85×10^5 . Samples for testing were machined from compression-molded bars, that had been annealed for 2 h at 95°C. Both the ABS and the SAN samples were carefully polished prior to testing.

The tension, compression, and fatigue tests were all performed at ambient temperature ($23 \pm 2^\circ\text{C}$) on an Instron servohydraulic unit. The samples for the compression tests were cylindrical with a diameter of 1.27 cm and a height of 2.54 cm. The samples for the tension and fatigue tests were generally of circular cross section with a diameter of 5.1 mm; but some tests were also run on samples of rectangular cross-section, with dimensions of 3.17×6.35 mm. The reduced gage length of the samples was 12.7 mm, but the effective gage length used to estimate strains from recorded displacements, was taken as double this value. The tension tests were run at variable strain rates, $\dot{\epsilon}$, ranging from 3.3×10^{-5} to $8.3 \times 10^{-2} \text{ s}^{-1}$. The fatigue tests were run both as a function of stress at fixed frequencies and as a function of frequency, ranging from 0.02 to 21 Hz, at a fixed stress amplitude. Generally 3–5 specimens were tested for each condition and cycles to fracture, N_f , determined by averaging individual $\log N_f$ values.

Estimates of the temperature rise, ΔT , in the fatigued samples, as a result of hysteretic heating, were made by means of a Barnes infrared sensor focused on the gage length of the samples. The fracture surface morphology of failed samples was examined by scanning electron microscopy (SEM) after first coating the fracture surfaces with a thin layer of gold-palladium.

RESULTS AND DISCUSSIONS

Deformation and Fracture Under Tensile Loading

Figure 1 shows typical tensile stress-strain curves for ABS and for the two grades of SAN. Both the SAN materials developed visible crazes during loading and the arrows on the curves represent the stress value at which surface crazes were first detected. The higher molecular weight SAN-C polymer, with a greater degree of chain entanglement between neighboring chains, has greater resistance to craze breakdown; and hence its fracture stress and fracture strain are somewhat higher than those of the lower molecular weight SAN-B polymer. The presence of craze deformation in SAN-type polymers, and also of fracture by craze breakdown, can be inferred from examination of fracture surfaces. An SEM scan of a portion of the fracture surface of an SAN-C sample is shown in Figure 2. A series of so-called mackerel bands, similar to those observed in PS,⁹ surround the fracture source. These arise as a result of unstable crack propagation, with the crack jumping periodically from one of the craze-bulk interfaces to the other and leaving behind on the fracture surface a series of craze layers.

The stress-strain response of the rubber-modified polymer is quite different.^{1,5} Whereas the SAN polymers show no yield maximum and essentially no reduction in cross-sectional area prior to fracture, ABS yields at a relatively low value of the applied tensile stress and a necked region develops and extends along the gage length. Direct evidence of the presence of intersecting shear bands, which give rise to the necking phenomenon, is given in Figure 3(a), which is an SEM scan of a portion of the free surface of a drawn sample. From TEM examination of drawn thin films, it has been suggested that the smaller size rubber particles in ABS give rise to localized shear deformation of the

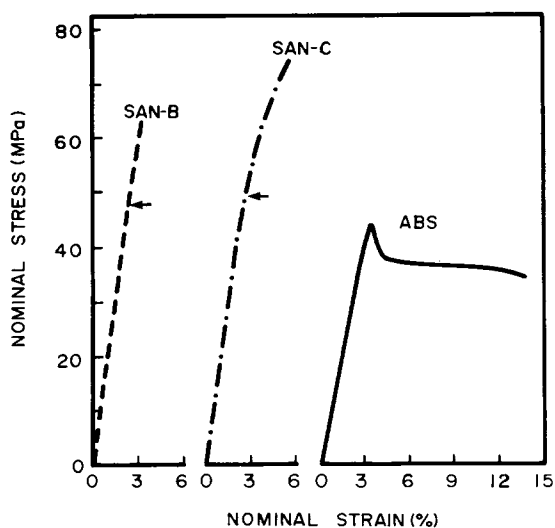


Fig. 1. Stress-strain curves of ABS, SAN-B ($M_w = 1.3 \times 10^5$) and SAN-C ($M_w = 1.85 \times 10^5$) Tests made at $\dot{\epsilon} = 3.3 \times 10^{-4} \text{ s}^{-1}$.

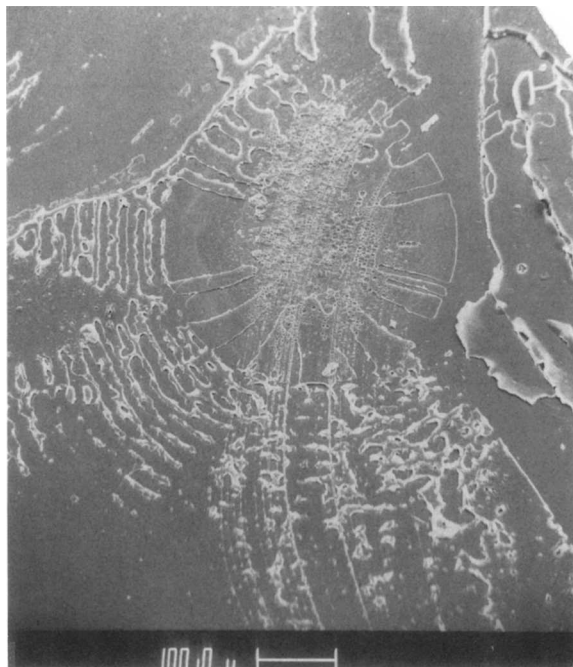
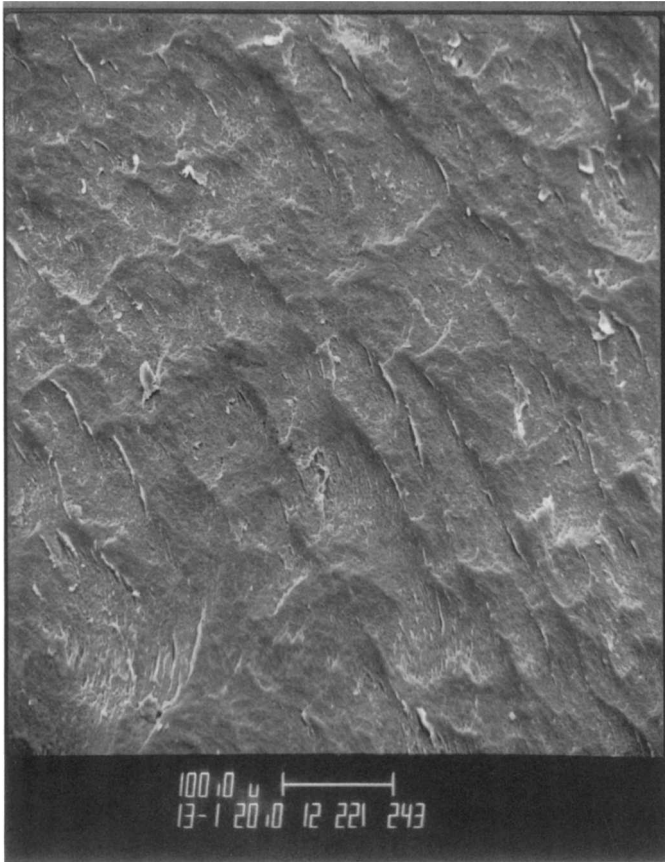


Fig. 2. SEM scan of part of fracture surface of an SAN-C sample fractured in tension.

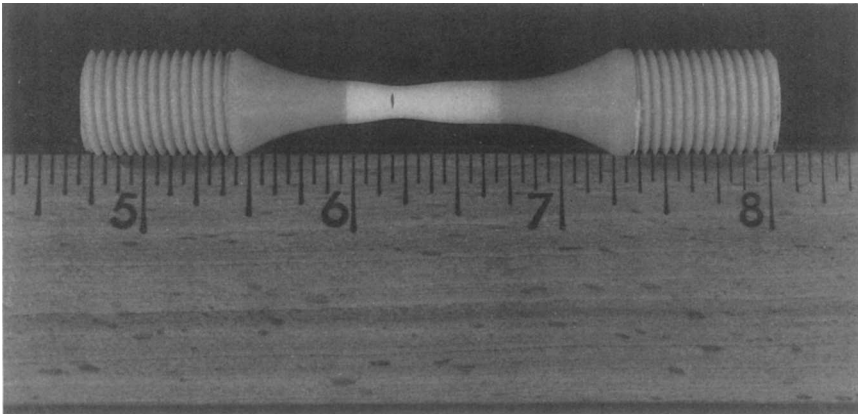
surrounding matrix while the larger size particles tend to promote crazing.¹⁰ It has also been observed that small grafted rubber particles ($< 0.5 \mu\text{m}$ in diameter) induce shear bands in polyvinylchloride (PVC).¹¹ The ABS material of this study possesses a fairly wide range of rubber particle size, hence we might expect to find not only shear bands but craze deformation as well.

Craze deformation, although readily seen in TEM scans of drawn thin films of ABS,^{8,10} is more difficult to detect in bulk samples of pigmented polymer. The presence of crazes is usually inferred from the stress whitening [Fig. 3(b)], that develops and intensifies as the yield strain is reached and exceeded. However, stress whitening can also arise from rubber particle cavitation and, in fact, is present in drawn samples of PVC which show little, if any, evidence of crazing.¹¹ Direct evidence of craze deformation in ABS is shown by Figure 4(a). This picture has been obtained by etching the free surface of a drawn sample, in the manner described by Bucknall,¹ and then examining the surface by scanning electron microscopy. As shown here, crazes in bulk specimens of ABS tend to be short and blunt. This probably occurs because of hinderance to growth by the presence of shear bands. Nevertheless, with continued strain, crack nucleation and development, as Figure 3(b) indicates, occurs within crazed material by fracture of craze fibrils.

The interior microstructure of a typical ABS craze is shown at higher magnification in Figure 4(b). Both intact craze fibrils, as well as some broken and retracted ones, are visible. These craze fibrils, which appear to be about $0.2 \mu\text{m}$ in diameter, are considerably larger than the craze fibrils observed in drawn thin films of ABS.⁸ Possibly some craze fibril coalescence has occurred in the bulk samples as a result of the etching treatment.

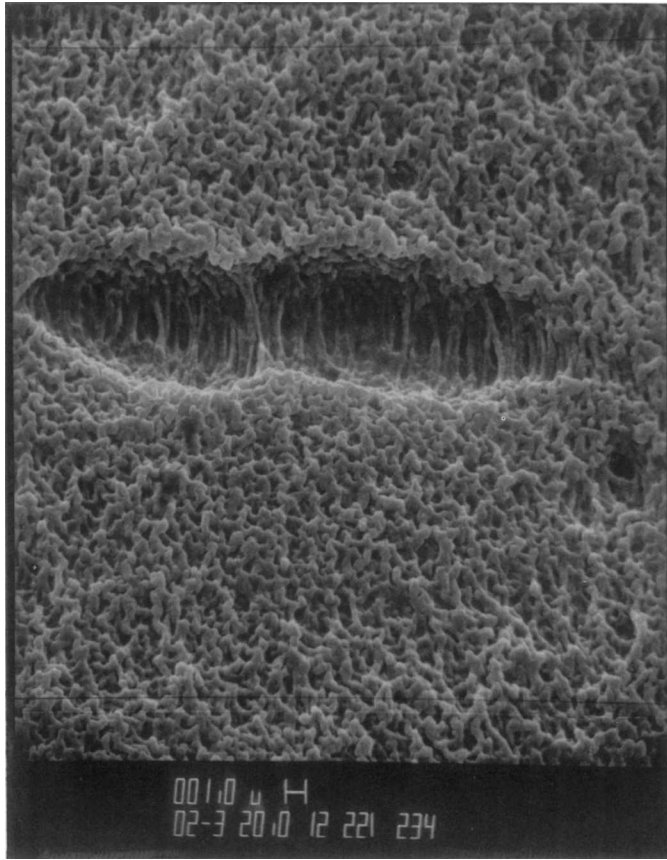


(a)

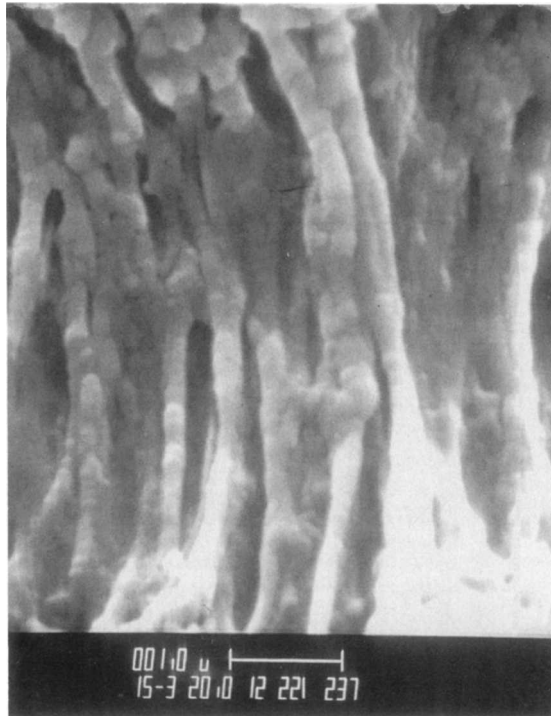


(b)

Fig. 3. (a) SEM scan showing shear bands in the free surface of a drawn ABS sample (b) Photo of drawn ABS sample showing zone of stress whitening and start of fracture. Scale shown is in inches.



(a)



(b)

Fig. 4. SEM scans of a portion of the free surface of a drawn sample of ABS after etching: (a) view of surface craze; (b) high magnification view of craze microstructure.

Deformation and Yield under Compressive Loading

Under compressive loading, both SAN and ABS samples undergo only shear yielding. Values of the compressive yield stress, σ_y^c , also obtained at a strain rate of $3.3 \times 10^{-4} \text{ s}^{-1}$, of the tensile yield (or fracture) stress, σ_y^T , and of the ratio of these two stresses are given in Table I for both of the SAN polymers and also for ABS. Inspection of the data given here show that the compressive yield stress of the rubber-modified polymer is less than half that of the SAN polymers. This large difference arises from several causes, viz., a reduced cross-sectional area of the rigid phase, the stress concentration effect of the rubber particles, and the overlapping of the stress fields from adjacent particles that result from the high volume concentration of the particles. The two SAN polymers, though differing in tensile strength, have essentially the same yield stress in compression, as shear yielding in polymers involves only small scale molecular motions,¹² and hence is unaffected by molecular weight.

Shear yielding in polymers is affected by the hydrostatic component of stress that is present. In many polymers, yielding is governed by a modified von Mises theory¹³ in which the octahedral shear stress, τ_{oct} , is given as a linear function of the mean stress, σ_m ,

$$\tau_{\text{oct}} = \tau_0 - \mu\sigma_m \quad (1)$$

where τ_0 and μ are material constants. This theory leads to the following equation for the ratio of the compressive to tensile yield stress

$$\sigma_y^c / \sigma_y^T = (\sqrt{2} + \mu) / (\sqrt{2} - \mu) \quad (2)$$

Since from our data, the yield stress ratio for ABS is 1.24, the value of the material constant μ is 0.15. Comparable values of this constant have been obtained for other polymers, viz., 0.16 for PMMA¹³ and 0.14 for poly(vinyl chloride).¹⁴ The yield stress ratio for the two SAN polymers is much higher than for ABS because, when these polymers are subject to tension, craze yielding and fracture intervene before the shear yield stress is reached (Fig. 1).

Influence of Strain Rate on Yield Stress and Fracture

The tensile yield stress of our compression-molded samples of ABS is shown as a function of strain rate in Figure 5. The yield stress is found to increase linearly with the log of the strain rate, as previously noted for injection-molded

TABLE I
Yield (or Fracture) Stress of ABS and SAN in Compression and Tension

Material	σ_y^c (MPa)	σ_y^T (MPa)	Ratio (σ_y^c / σ_y^T)
ABS	52.7	42.4	1.24
SAN-B	117	63.1	1.85
SAN-C	118	73.8	1.60

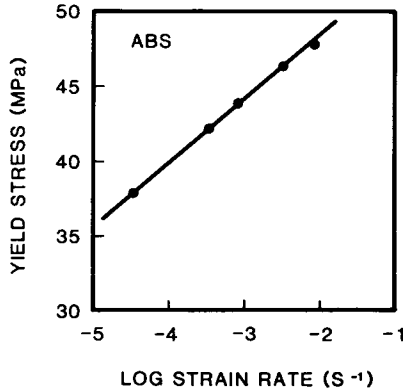


Fig. 5. Tensile yield stress of ABS vs. log (strain rate).

samples of ABS by Truss and Chadwick.¹⁵ The test results can be described by an Eyring type rate equation

$$\sigma_y = \frac{\Delta H}{v} + \frac{2.3kT}{v} \log(\dot{\epsilon}/A) \quad (3)$$

where ΔH is the activation energy, v the activation volume, k the Boltzmann constant, T the temperature in degrees Kelvin, and A is a constant. From the measured slope of the line in Figure 5, the activation volume is found to be 2.2 nm^3 . This value is in good agreement with reported values of 2.3 nm^3 for a pigmented, medium molecular weight grade of ABS¹⁵ and of 2.2 nm^3 for a transparent grade of ABS.¹⁶

Tensile fracture surfaces have been examined by SEM at both low and high strain rates. A typical fracture surface obtained at a low strain rate is shown in Figure 6(a). Most of the surface is transverse to the stress axis, except for a rather large cone-shaped cavity that developed about an internal impurity particle. In this region, the opposite fracture surface, shown in Figure 6(b), is a mirror image of that shown in Figure 6(a). Both surfaces show a conical depression surrounding a relatively large inclusion, which, in this specimen has a size of about $70 \mu\text{m}$. Double cone-shaped cavities, that have developed from large inclusions, have also been observed in injection-molded samples of ABS of varying rubber content.¹⁷ It appears from Figure 6 that the impurity particle that gave rise to the double cone-shaped cavity has itself been fractured as remnants of the particle are visible, especially at higher magnification, on both of the opposite fracture surfaces.

The internal cone-shaped cavities in ABS appear to be somewhat analogous to the surface diamond-shaped cavities observed in ductile fracture of poly(vinyl)chloride and other polymers.¹⁸ In the formation of the cavities, some localized shear deformation has occurred. However, the generally planar nature of the remainder of the fracture surface, and the more intense stress-whitening in this region, suggest that the fracture crack has here propagated through the numerous small crazes that tend to generate ahead of the crack tip in the vicinity of the dispersed rubber particles. A high magnification scan

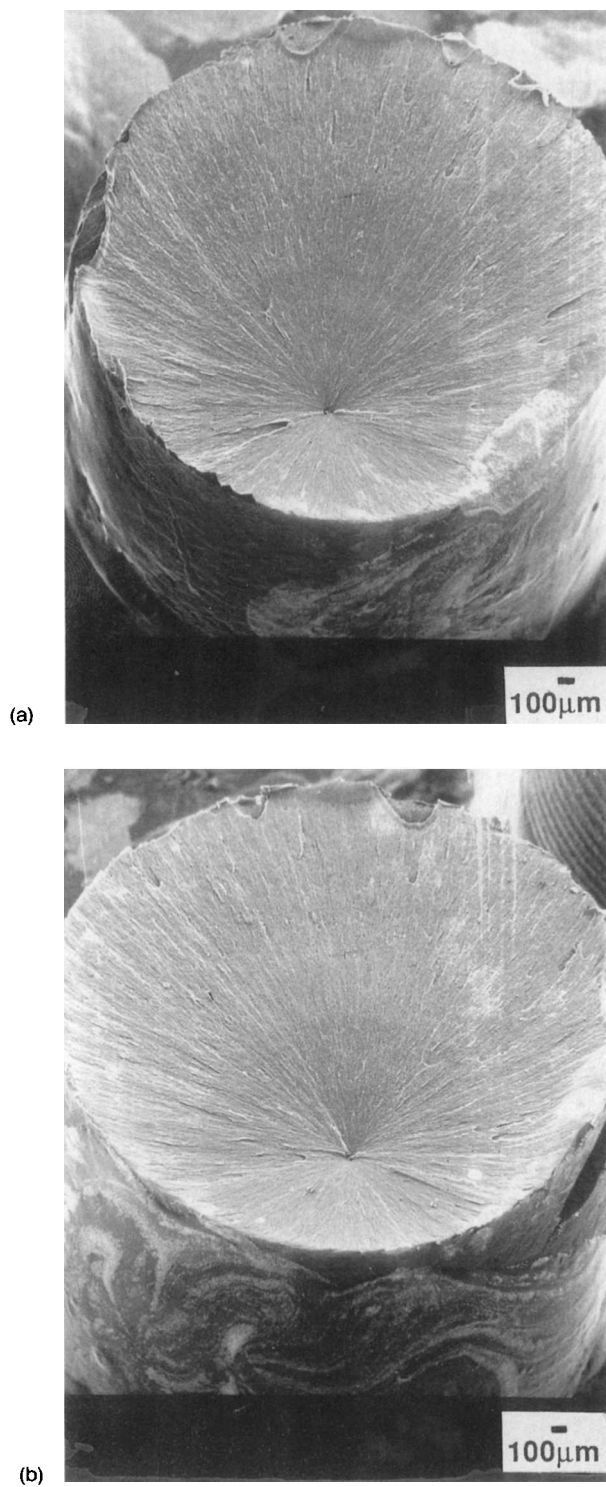


Fig. 6. SEM scans of the tensile fracture surface of an ABS sample tested at $\dot{\epsilon} = 8.3 \times 10^{-5} \text{ s}^{-1}$: (a) one fracture surface; (b) opposite fracture surface.

taken in the region near to an impurity particle, is shown in Figure 7. It appears that many of the rubber particles have cavitated, as a result of the hydrostatic tension existing in the region ahead of the crack tip. The many small cavities that are visible are comparable in size to the dispersed rubber particles. The SEM scan shows that the matrix material between the particles has been plastically deformed and, in this slow-growth region near to the fracture source, there is little, if any, alignment of the drawn matrix material along the crack propagation direction.

At higher strain rates, there is a tendency for fracture to develop from a surface source, which may be a craze or a small diamond-shaped cavity. Figures 8(a) and 8(b) show opposite fracture surfaces of a sample tested at $3.3 \times 10^{-3} \text{ s}^{-1}$. The primary crack has progressed gradually inward from its surface origin in a flaw or craze. Numerous conical features are seen on the fracture surface. These result from interaction between the advancing primary crack and the secondary cracks, initiated at slightly different elevations, at small impurity particles. Secondary fracture parabolas have also been noted on the tensile fracture surface of injection-molded ABS samples.¹⁷ Also visible in Figure 8 is an internal cavity that has resulted from independent crack development and growth about a large inclusion.

A high magnification scan of the fracture surface of another ABS sample, that has been deformed at a high strain rate, is shown in Figure 9. This sample also exhibited initial crack development from an external surface source and



Fig. 7. SEM high magnification view of an ABS fracture surface taken near to an internal source. Sample tested at $\dot{\epsilon} = 8.3 \times 10^{-4} \text{ s}^{-1}$.

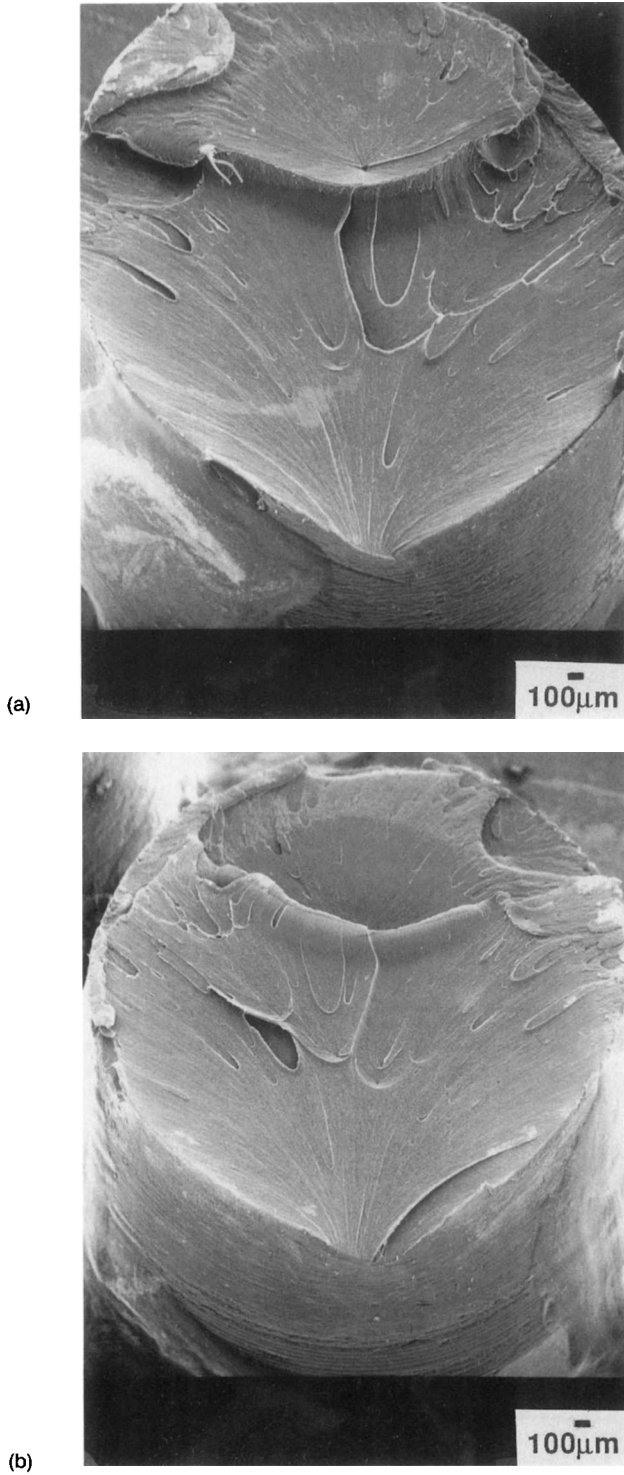


Fig. 8. SEM scans of the tensile fracture surface of an ABS samples tested at $\dot{\epsilon} = 3.3 \times 10^{-3} \text{ s}^{-1}$: (a) one fracture surface; (b) opposite fracture surface.

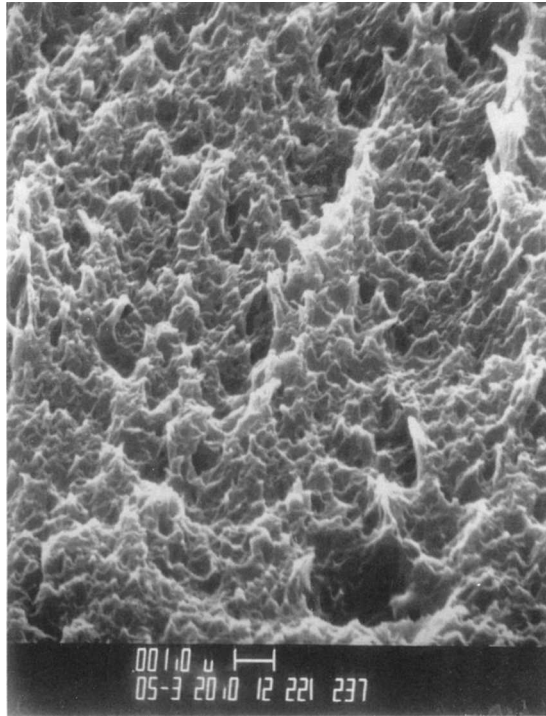


Fig. 9. SEM high magnification view of an ABS fracture surface taken away from an external, surface source. Sample tested at $\dot{\epsilon} = 8.3 \times 10^{-2} \text{s}^{-1}$.

later crack initiation and development from an internal source. Figure 9 shows only a portion of the primary crack domain taken away from the surface source. In this fast crack growth region, many matrix fibrillar elements are seen and these are aligned to some extent along the crack propagation direction. The many voids seen here, which again are comparable in size to the rubber particles, probably arise from cavitation of the rubber particles. TEM studies of deformed thin films of ABS show that rubber particle cavitation occurs readily in this polymer upon tensile straining.^{8,10}

Deformation and Fracture Under Alternating Stress

When polymers fracture under alternating stress conditions, they do so in a macroscopically brittle manner, even though the same polymer might be quite ductile in a simple tension test. ABS is no exception. Even when it is cycled at moderate stress amplitudes that are well below the tensile yield stress, but above some minimum value, it will fail after some critical number of fatigue cycles without significant plastic deformation or necking and without extensive stress whitening.^{5,6} Nevertheless, as observations of hysteresis loop geometry show, both localized shear deformation and crazing do occur prior to the fatigue fracture.^{5,19,20}

Some fatigue test data obtained on ABS, and on two grades of SAN, at two different stress amplitudes and at a frequency of 21 Hz, are given in Table II

TABLE II
Cycles to Fracture and Temperature Rise in ABS and SAN at 21 Hz

Stress amplitude (MPa)	ABS		SAN-B		SAN-C		ABS (interrupted)	
	N_f	ΔT (°C)	N_f	ΔT (°C)	N_f	ΔT (°C)	N_f	ΔT (°C)
27.6	5050	24	14,800	5	22,900	—	12,600	5
31.0	2390	35	6610	6.5	7580	7.3	5640	5

The columns labeled N_f give the average number of cycles to fatigue failure and the columns labeled ΔT give the maximum specimen temperature rise, resulting from hysteresis effects, prior to fracture. The test results show that fatigue lifetime, as denoted by the average number of cycles to failure, is 175% to 350% higher for the SAN polymers than for ABS. A principal reason for this behavior is that the dispersed rubber particles, by acting as stress concentrators, cause craze development and breakdown to occur sooner than in the unmodified polymer.⁶ Hence, even though the particles may give an increased resistance to crack propagation,³ the craze/crack initiation phase dominates behavior and total lifetime is reduced. It is interesting to note that rubber modification of polystyrene also reduced fatigue life and that this reduction is essentially proportional to the rubber content.²¹

Another reason for the poorer fatigue performance of ABS compared with SAN is that thermal effects due to hysteresis are more severe. As Table II shows, the temperature rise in the unmodified polymer falls in the range 5–7°C, while the rise in the ABS samples is from 24 to 35°C. To investigate the significance of such disparate thermal effects on fatigue performance, a new series of tests were run and the data obtained are given in the last two columns of Table I. In this series of experiments, the tests were interrupted whenever the temperature of the ABS samples reached 5°C above ambient; and cycling was renewed after the samples had cooled to room temperature. Interruptions and renewals were continued until fracture. The data obtained show that cycles to fracture for the ABS samples in these interrupted tests are now closer in value to the lifetimes observed in the unmodified SAN samples. Disparate thermal effects are thus partly responsible for the inferior fatigue performance of the rubber-modified polymer.

A third reason why the rubber-modified polymer fails sooner than the unmodified polymer when both are fatigue tested at the same stress amplitude is that the applied stress is much closer in value to the tensile yield or fracture stress in ABS than it is in SAN. For example, at the stress amplitude of 27.6 MPa, the relative stress ratio, i.e., the ratio of the stress amplitude to the tensile yield or fracture stress, is about 0.65 for ABS vs. 0.44 for SAN-B. If the fatigue tests were conducted at the same relative stress ratio, instead of at the same nominal stress amplitude, then ABS would be superior in fatigue resistance to SAN.⁷ To illustrate this, we note that when ABS is tested at 20.7 MPa and SAN-B is tested at 31 MPa, the relative stress ratio for both materials will be the same, viz., 0.49. Under this condition, the average number of cycles to failure, for tests at 21 Hz, is found to be 34,100 for ABS as compared with 5510 cycles for SAN-B. As another illustration, the extrapolated relative stress ratio,

below which no failure is expected to occur within 10^6 cycles, is estimated as 0.37 for ABS vs. 0.29 for SAN-B. The superior performance of the rubber-modified polymer when tested at the same relative stress ratio is attributed to an enhanced resistance to crack propagation offered by the dispersed rubber particles.

To determine how the fatigue fracture surface morphology varies upon rubber modification, we compare the fracture surfaces of samples of the unmodified polymer with those of the rubber-modified polymer tested under the same conditions (27.6 MPa and 21 Hz). A typical fatigue fracture surface for an SAN-C specimen is shown in Figure 10. The fracture surface consists of two distinct regions, one a smooth slow-growth region surrounding the fracture origin, which is here a surface craze, and the other a rough region of rapid crack propagation. The fatigue fracture surface for the lower molecular weight SAN-B sample is similar, except that the size of the slow-growth region is smaller and, in this region, a series of discontinuous crack growth (DCG) bands, indicative of periodic crack propagation in essentially a single craze plane, are present.⁵ The absence of such bands in the higher molecular weight SAN-C polymer is attributed to the presence of multiple crazes at the crack tip. The greater stability of higher molecular weight polymer also leads to the absence of DCG bands in high-molecular weight grades of PVC³ and of PMMA.²²

In contrast to SAN, the fatigue fracture surface of ABS, tested under the same conditions, shows no clearcut transition between a slow-growth and a

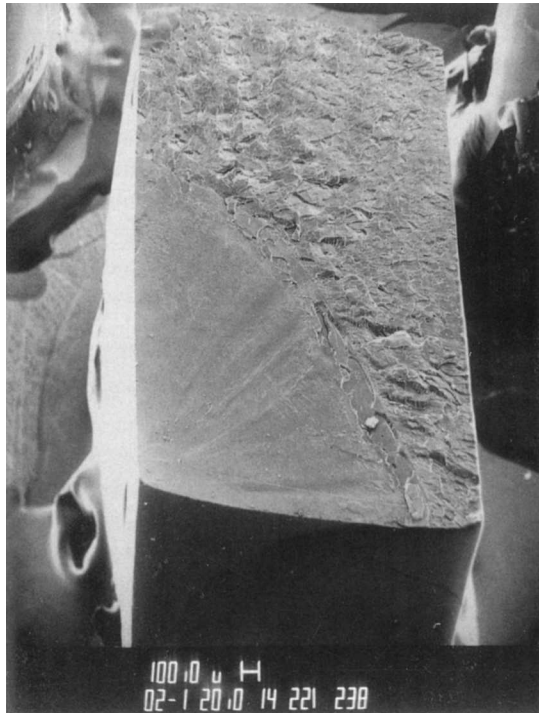


Fig. 10. SEM scan of the fatigue fracture surface of an SAN-C sample tested at 27.6 MPa and 21 Hz.

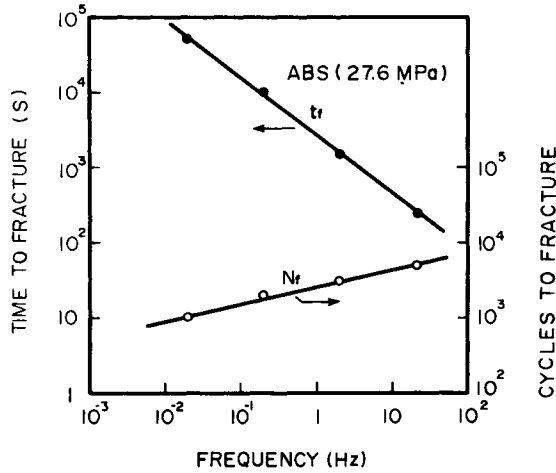


Fig. 11. Time to fracture, t_f , and cycles to fracture, N_f , vs. test frequency for ABS samples tested at 27.6 MPa.

fast-growth region and the entire fracture surface (see Fig. 49a of Ref. 5) is comparatively smooth. There is also no evidence of any cone-shaped cavity such as occurs in tensile fracture of ABS. At higher magnification, there is evidence of considerable localized plastic deformation of the matrix material despite the macroscopic brittle nature of the fatigue fracture. Also seen are many small cavities which probably arise from cavitation of the rubber particles under the high triaxial stress field existing near to the crack tip.

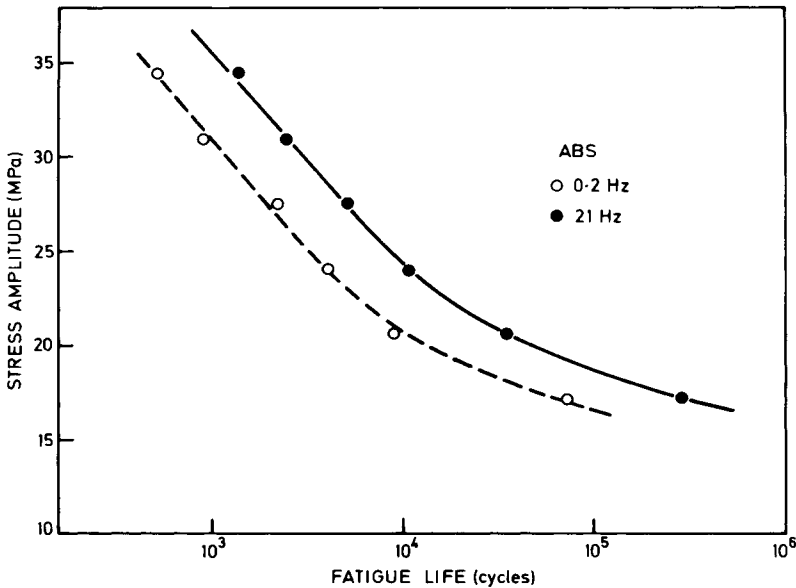


Fig. 12. S-N curves of ABS at 0.2 and 21 Hz.

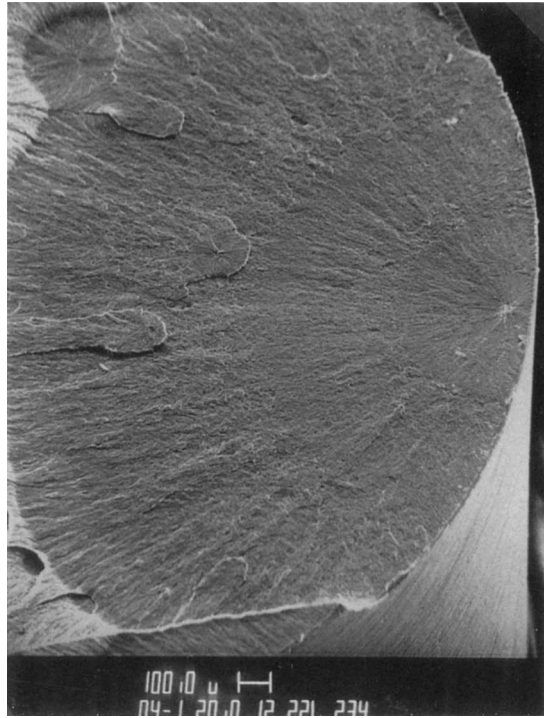


Fig. 13. SEM scan of slow-growth portion of the fatigue fracture surface of an ABS sample tested at 27.6 MPa and 0.02 Hz.

The Influence of Frequency on Fatigue Performance of ABS

The average time to fracture, t_f , as well as the average number of cycles to fracture, N_f , have been determined over a 1000-fold range of test frequency for ABS samples subject to a stress amplitude of 27.6 MPa. The results are presented in Figure 11. On this log-log plot, the time to failure is seen to decrease linearly with increase of frequency. It has been shown that if fatigue fracture is a cycle-dependent process, the slope of this graph should be -1 , while if it is a result of a cumulative damage process, in which the damage rate is a function of stress magnitude, it should be zero.²³ The actual slope is -0.77 . Hence fatigue failure in ABS is not in agreement with either hypothesis but it is more in accord with a cycle-dependent model.

It is evident from Figure 11 that N_f is not independent of test frequency, as one would expect for a cycle-dependent process. However, its variation with frequency is a relatively modest one, *viz.*, about an increase of a factor of 5 for a 1000-fold increase in frequency. This increase is much less, for example, than that observed in another rubber-modified polymer, HIPS, where a 50-fold rise in N_f was noted over the same frequency range for samples tested at 17.6 MPa.⁵ The relatively modest increase in cycles to fracture for ABS with increasing frequency is also evident from Figure 12, where we compare S-N data obtained at 0.2 Hz⁵ with that obtained at 21 Hz.⁶ At all stress amplitudes, the increase in cycles to fracture over a two-decade rise in frequency is only about a factor



Fig. 14. SEM scan of the fatigue fracture of an ABS sample tested at 27.6 MPa and 0.2 Hz.

of 3. Over the same frequency range, both HIPS and PS increase by over a decade.

The fracture surface morphology of ABS varies appreciably with stress magnitude and, to some extent, with test frequency. At high stresses, above about 70% of the tensile yield stress, there is no single fracture initiation site and the entire fracture surface is very rough.⁵ At moderate stress amplitudes, between about 50 to 70% of the yield stress and at low test frequencies fracture seems to develop from an internal site, such as an inclusion or impurity particle. This is evident from Figure 13, which is a view of part of the fatigue fracture surface for a sample tested at 0.02 Hz and 27.6 MPa. The initiation site is clearly an internal heterogeneity and, in the slow-growth region surrounding the fracture source, several DCG bands are present. The DCG bands arise, as discussed by Hertzberg and Manson,³ when the resistance to crack penetration of the growing craze, or crazes, ahead of the crack tip is so reduced by fatigue induced damage that the crack jumps forward through the damaged material and again arrests. The bands are not as well defined in this rubber-modified polymer as they are in homopolymers. The reason may be that small rubber particles induce both crazes and shear bands in the surrounding matrix and the advancing crack has to pass through these localized deformation zones situated on different planes.

In some specimens tested at low frequency, several internal fracture sites may be activated. This is shown in Figure 14 for a sample tested at the same stress level of 27.6 MPa but at 0.2 Hz. Separate crack systems have developed from each site and final fracture has then resulted from tearing of the connecting

material lying between the separate crack systems. From comparison of the fracture surfaces of samples tested at low frequency, as shown in Figures 13 and 14, with those fractured at comparable stress but at the higher frequency of 21 Hz,⁶ it appears that when frequencies are low—and lifetime to fracture long—fatigue cracks develop from internal inhomogeneities and generally one, or more, smooth, slow-growth regions and a rougher fast-growth region are present on the fracture surface. But when the test frequency is high, the fatigue crack tends to initiate from surface flaws and advances transversely across the entire specimen. It is interesting to note that somewhat similar changes in the location of the fracture initiation site were observed on tensile fracture surfaces by changing from a low to a high strain rate. This may be related to the fact that with increasing strain rate the contribution of crazing to the total deformation rises while that of shear reduces.^{15,24}

CONCLUSIONS

In ABS specimens subject to tensile strain, direct evidence is given of both shear yielding and crazing while only crazing is seen in the unmodified SAN polymer.

The tensile yield stress of compression-molded specimens of ABS varies with strain rate in accord with the Eyring rate equation and the activation volume involved is estimated to be 2.3 nm^3 .

At low strain rates, fracture occurs by crack propagation from the edge of one, or several, developing double cone-shaped cavities that have formed around internal impurity sites. In contrast, at high strain rates, fracture usually develops from a surface flaw by crack initiation and propagation in crazed material.

Under alternating stress conditions, the second-phase particles in ABS cause earlier craze and crack nucleation and greater hysteretic heating; and both of these effects contribute to a reduction in the average fatigue life, at a given stress amplitude, as compared to that of SAN.

The time to fracture of ABS specimens under fatigue conditions decreases significantly with increase of frequency while cycles to fracture increase at a modest rate. Fracture tends to develop, at low frequency, from internal impurity sites and, at high frequency, from breakdown of surface-induced crazes.

This investigation was supported, in part, by the Division of Material Research of the National Science Foundation. We also wish to thank J. Trent for his assistance with the TEM measurements.

References

1. C. B. Bucknall, *Toughened Plastics*, Applied Science, London, 1977.
2. A. J. Kinloch and R. J. Young, *Fracture Behavior of Polymers*, Applied Science, London, 1983.
3. R. W. Hertzberg and J. A. Manson, *Fatigue of Engineering Plastics*, Academic Press, New York, 1980.
4. Der-jin Woan, M. Mabibullah, and J. A. Sauer, *Polymer*, **22**, 699 (1981).
5. J. A. Sauer and C. C. Chen, *Adv. Polym. Sci.*, **52/53**, 169 (1983).
6. J. A. Sauer and C. C. Chen, *Polym. Eng. Sci.*, **24**, 786 (1984).
7. J. A. Sauer and C. C. Chen, Intern. Conf. on Toughening of Plastics-II, Paper No. 26, Plastics and Rubber Inst., London, 1985.

8. J. S. Trent, Ph.D. dissertation, Rutgers University, 1983.
9. J. Murray and D. Hull, *J. Polym. Sci. Part A-2*, **8**, 583 (1970).
10. A. M. Donald and E. J. Kramer, *J. Mater. Sci.*, **17**, 1765 (1982).
11. H. Brauer, F. Haaf, and J. Stabenow, *J. Macromol. Sci.*, **B14**, 387 (1977).
12. A. S. Argon and M. I. Bessonov, *Phil. Mag.*, **35**, 917 (1977).
13. S. S. Sternstein, in *Polymeric Materials*, American Society of Metals, New York, p. 369.
14. J. A. Sauer, K. D. Pae, and S. K. Bhateja, *J. Macromol. Phys.*, **B8**, 631 (1973).
15. R. W. Truss and G. A. Chadwick, *J. Mater. Sci.*, **11**, 111 (1976).
16. R. W. Truss and G. A. Chadwick, *J. Mater. Sci.*, **11**, 1385 (1976).
17. R. W. Truss and G. A. Chadwick, *J. Mater. Sci.*, **12**, 503 (1977).
18. P. L. Cornes, K. Smith, and R. H. Haward, *J. Polym. Sci. Phys. Ed.*, **15**, 955 (1977).
19. C. B. Bucknall and W. W. Stevens, *J. Mater. Sci.*, **15**, 2950 (1980).
20. C. B. Bucknall and A. Marchetti, *Polym. Eng. Sci.*, **24**, 535 (1984).
21. J. A. Sauer, J. Trent, and C. C. Chen, *Polym. Eng. Sci.*, **29**, 69 (1989).
22. C. C. Chen, J. Shen, and J. A. Sauer, *Polymer*, **26**, 89 (1985).
23. G. B. McKenna and R. W. Penn, *Polymer*, **21**, 213 (1980).
24. R. N. Haward and C. B. Bucknall, *Pure & Appl. Chem.*, **46**, 227 (1976).

Received April 24, 1989

Accepted August 23, 1989